This document is a preprint of: P. Neuhaus, M. Dorpinghaus, H. Halbauer et al., "Sub-THz Wideband System Employing 1-bit Quantization and Temporal Oversampling," in Proceedings of IEEE International Conference on Communications (ICC 2020), Dublin, Ireland, (pp. 1-7), Jun 2020. DOI:10.1109/ICC40277.2020.9148753

Sub-THz Wideband System Employing 1-bit Quantization and Temporal Oversampling

Peter Neuhaus*, Meik Dörpinghaus*, Hardy Halbauer†, Stefan Wesemann†,
Martin Schlüter*, Florian Gast*, and Gerhard Fettweis*
*Vodafone Chair Mobile Communications Systems, Technische Universität Dresden, Dresden, Germany
{peter_friedrich.neuhaus, meik.doerpinghaus, martin.schlueter, florian.gast, gerhard.fettweis}@tu-dresden.de
† Nokia Bell Labs, Stuttgart, Germany. {hardy.halbauer, stefan.wesemann}@nokia-bell-labs.com

***Abstract*—Wireless communications systems beyond 5G are foreseen to utilize the large available bandwidths above 100 GHz. However, the power consumption of analog-to-digital converters (ADCs) for such systems is expected to be prohibitively high, because it grows quadratically with the sampling rate for high amplitude resolutions. Shifting the resolution from the amplitude to the time domain, i.e., by reducing the amplitude resolution and by employing temporal oversampling w.r.t. the Nyquist rate, is expected to be more energy efficient.**

To this end, we propose a novel low-cost sub-terahertz system employing zero crossing modulation (ZXM) transmit signals in combination with 1-bit quantization and temporal oversampling at the receiver. We derive and evaluate new finite-state machines for efficient de-/modulation of ZXM transmit signals, i.e., for efficient bit sequence to symbol sequence de-/mapping. Furthermore, the coded performance of the system is evaluated for a wideband line-of-sight channel.

***Index Terms*—1-bit, quantization, oversampling, faster-than-Nyquist signaling, runlength-limited sequences**

I. Introduction

Wireless communications systems beyond 5G are foreseen to utilize available frequency bands in the millimeter wave (mmWave) and terahertz (THz) regime in order to cope with the ever-increasing demand for higher data rates. Especially the *sub-THz* band from 100 GHz to 300 GHz provides large amounts of free spectrum [1]. However, the power consumption of the analog-to-digital converter (ADC) is becoming a major issue for such wideband systems, because it grows quadratically with the sampling rate for high amplitude resolutions [2]. At the same time, *time-domain* resolution is becoming superior to *amplitude-domain* resolution in modern nanometer-scale CMOS processes [3], [4]. This is mainly caused by reduced supply-voltages, which leave less voltage-headroom for sophisticated amplitude processing. Consequently, it is expected to be more energy efficient to shift the resolution from the amplitude to the time-domain, i.e., by reducing the amplitude resolution and by employing temporal oversampling at the ADC. Furthermore, reducing the amplitude resolution to just 1-bit seems especially promising because it neither requires an automatic gain control nor a linear low-noise amplifier, since all magnitude information is lost after 1-bit quantization.

In this work we aim to design a low-cost wideband radio access technology for sub-THz bands. To this end, we propose to employ 1-bit quantization and temporal oversampling at the receiver, which potentially reduces the ADC power consumption significantly. The transmit signal is designed matched to the 1-bit temporal oversampling receiver, by encoding the information in the distances between zero crossings; a concept which is denoted as zero crossing modulation (ZXM) [5]. The high path loss at the considered frequencies requires the use of antenna arrays at both the transmitter and the receiver. In this work we focus on the receiver, which is assumed to be equipped with an analog phase-shifter network (PSN), a single RF chain, and a single 1-bit ADC for reduced cost and power consumption. Due to the large bandwidth, the received signal can change considerably while propagating across the antenna array at the receiver for the considered wideband channels in the mmWave and sub-THz bands. This effect is known as spatial-wideband effect (SWE) and has to be taken into account at the receiver [6].

Lower bounds on the spectral efficiency for systems employing 1-bit quantization and temporal oversampling are computed numerically in [7] for an additive white Gaussian noise (AWGN) channel. The achievable rate for a 1-bit quantized continuous-time AWGN channel is investigated in [8], which can be interpreted as the limiting case of infinite oversampling. The spectral efficiency of multiple-input multiple output channels with 1-bit quantization and temporal oversampling is investigated in [9]. Synchronization for systems employing 1-bit quantization and temporal oversampling is studied in [10], bounds on the channel parameter estimator performance are evaluated in [11] and [12]. 1-bit quantized temporal and spatial oversampling, i.e., using multiple antennas, where each antenna is equipped with a single 1-bit ADC employing Nyquist rate sampling, are compared in [13] for a wideband line-of-sight (LOS) channel. Moreover, a massive MIMO system employing 1-bit quantization and temporal oversampling is studied in [14]. Soft-output detection algorithms for frequency selective mmWave MIMO systems with low-precision ADCs employing Nyquist rate sampling are investigated in [15].

The main contributions of this work are as follows: *i*) design and modeling of a wideband sub-THz system employing 1-bit quantization and temporal oversampling at the receiver, *ii*) derivation of two finite-state machine (FSM) runlength-limited (RLL) sequence encoders for efficient encoding and soft-input soft-output decoding and *iii*) a coded performance evaluation of the proposed system for a wideband LOS channel.

This document is a preprint of: P. Neuhaus, M. Dorpinghaus, H. Halbauer et al., "Sub-THz Wideband System Employing 1-bit Quantization and Temporal Oversampling," in Proceedings of IEEE International Conference on Communications (ICC 2020), Dublin, Ireland, (pp. 1-7), Jun 2020. DOI:10.1109/ICC40277.2020.9148753

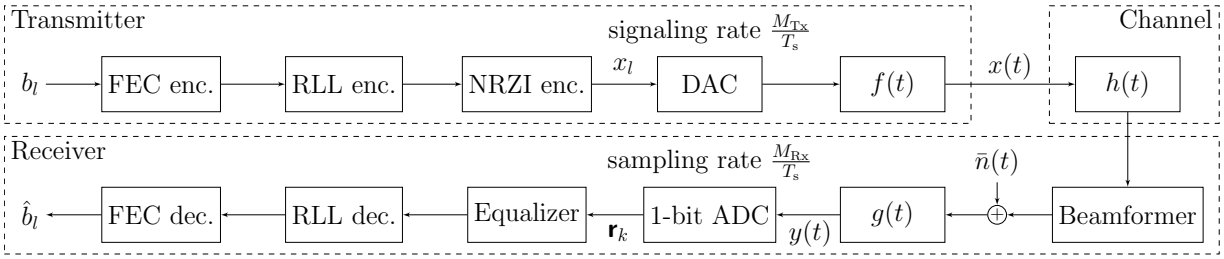

Fig. 1. Overview on the system model, where b_l corresponds to the input bits to be transmitted and $\hat{b}_l$ to their estimates at the receiver.

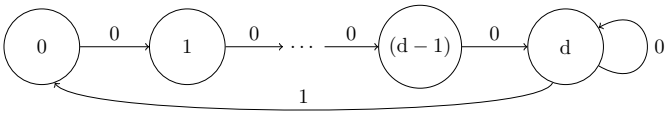

Fig. 2. State machine describing $(d, k = \infty)$ constrained sequences.

II. System Model

An overview on the considered system model is provided in Fig. 1. Transmit and receive filters are assumed to be root-raised-cosine (RRC) filters, denoted by $f(t)$ and $g(t)$, respectively. Transmit beamforming is omitted because this work focuses on the receiver design. Note that we assume perfect synchronization and channel state information at the receiver throughout this work.

A. Transmit Signal

The transmitter employs ZXM, which is a modulation matched to receivers employing 1-bit quantization and temporal oversampling [5]. It is motivated by the fact that a receiver employing 1-bit quantization can effectively only determine when the received signal has a zero crossing, i.e., when the signal amplitude changes from above zero to below zero or vice versa. Hence, it is intuitive to encode the information in the distances between zero crossings instead of the amplitude.

1) Runlength-Limited Sequences: One practical way of generating ZXM transmit signals is to utilize RLL sequences [16]. RLL sequences can be constructed from (d, k) sequences, which are constrained binary sequences in which every 1 has to be followed by at least d and at most k 0s. The k constraint is omitted here, i.e., $k = \infty$, which maximizes the entropy rate. The constraint is illustrated as a FSM in Fig. 2. A RLL sequence can then be constructed by realizing an amplitude transition at every 1 in the (d, k) sequence, as shown in the following example:

$$\begin{aligned}(d,k)\quad &\bar{\mathbf{a}}^m = [\ldots,\ 0,\ 1,\ 0,\ 1,\ 0,\ 0,\ 1,\ldots]^T\\ \text{RLL}\quad &\mathbf{a}^m = [\ldots,-1,\ 1,\ 1,-1,-1,-1,\ 1,\ldots]^T,\end{aligned}$$

where $\mathbf{a}^m \in \{-1,+1\}^m$ and $m \in \mathbb{N}_+$ denotes the length of the sequence. The mapping from (d, k) to RLL sequences is known as non-return-to-zero-inverse (NRZI) encoding. Note that the d constraint effectively specifies the minimum distance between two amplitude transitions.

A complex-valued transmit sequence can be constructed from two real-valued independently modulated RLL sequences $\mathbf{a}^m, \mathbf{b}^m \in \{-1,+1\}^m$ as

$$\mathbf{x}^m = \frac{1}{\sqrt{2}}\left(\mathbf{a}^m + j\,\mathbf{b}^m\right). \tag{1}$$

The lth element of $\mathbf{x}^m$ is denoted as $x_l \in \mathcal{X} = \left\{\frac{1+j}{\sqrt{2}}, \frac{1-j}{\sqrt{2}}, \frac{-1+j}{\sqrt{2}}, \frac{-1-j}{\sqrt{2}}\right\}$. Encoding of information bits onto RLL sequences is discussed in Sec. III. Using this, the continuous-time transmit signal is given by

$$\tilde{x}(t) = \sum_{l=1}^{m} x_l f\left(t - lT_{\mathrm{s}}\right), \tag{2}$$

where T_{s} denotes the Nyquist interval.

2) Faster-than-Nyquist Signaling: Combining (2) with faster-than-Nyquist (FTN) signaling [17], increases the time-domain resolution at the transmitter and allows to produce zero crossings on a finer grid. This can be used to increase the achievable rate as proposed in [7]. The resulting modified transmit signal is given by

$$x(t) = \sum_{l=1}^{m} x_l f\left(t - \frac{lT_{\mathrm{s}}}{M_{\mathrm{Tx}}}\right), \tag{3}$$

where $M_{\mathrm{Tx}} \in [1, \infty)$ denotes the FTN signaling factor. Note that increasing the signaling rate increases the throughput, but comes at the cost of self-introduced intersymbol interference (ISI). However, the amount of ISI can be controlled by the d constraint of the RLL code.

B. Channel Model

We consider a single antenna transmitter and a receiver which is equipped with a uniform rectangular array (URA) with a total of $N = N_{\mathrm{h}} \cdot N_{\mathrm{v}}$ antennas, where N_{h} and N_{v} denote the number of horizontal and vertical antennas, respectively. The channel is assumed to be LOS and characterized by the angles-of-arrival (AoAs), i.e., the azimuth angle $\phi \in [-\pi, \pi)$ and the elevation angle $\theta \in [-\frac{\pi}{2}, \frac{\pi}{2})$. Under the far-field assumption, the propagation delay between the nth receive antenna and the center of the URA can be defined as

$$\tau_n = \frac{1}{c}\mathbf{k}(\phi,\theta)^T\left(\mathbf{u}_n - \bar{\mathbf{u}}\right), \quad n \in \mathcal{N} = \{1,\ldots,N\}, \tag{4}$$

where c denotes the speed of light,

$$\mathbf{k}(\phi,\theta) = \begin{bmatrix}\cos\theta\cos\phi\\ \cos\theta\sin\phi\\ \sin\theta\end{bmatrix} \tag{5}$$

This document is a preprint of: P. Neuhaus, M. Dorpinghaus, H. Halbauer et al., "Sub-THz Wideband System Employing 1-bit Quantization and Temporal Oversampling," in Proceedings of IEEE International Conference on Communications (ICC 2020), Dublin, Ireland, (pp. 1-7), Jun 2020. DOI:10.1109/ICC40277.2020.9148753

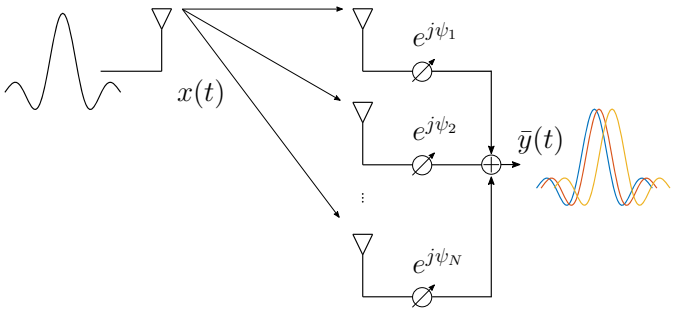

Fig. 3. The wideband received signal is added incoherently after passing through the PSN, because delays are not compensated.

corresponds to the wave vector up to a scaling factor, and $\mathbf{u}_n \in \mathbb{R}^3$ and $\bar{\mathbf{u}} \in \mathbb{R}^3$ define the position of the nth antenna and the center of the URA, respectively. They are given by

$$\mathbf{u}_n = \begin{bmatrix} 0 \\ \mathrm{mod}\,(n-1, N_\mathrm{h})\; d_\mathrm{h} \\ \lfloor (n-1)/N_\mathrm{h} \rfloor\, d_\mathrm{v} \end{bmatrix}, \quad \bar{\mathbf{u}} = \begin{bmatrix} 0 \\ \frac{(N_\mathrm{h}-1)d_\mathrm{h}}{2} \\ \frac{(N_\mathrm{v}-1)d_\mathrm{v}}{2} \end{bmatrix}, \tag{6}$$

where d_h and d_v denote the horizontal and vertical antenna spacing, respectively. Then, in baseband the wideband channel from the transmitter to the nth receive antenna is given by

$$h_n(t) = \delta\left(t - \tau_n\right) e^{-j2\pi f_\mathrm{c} \tau_n}, \quad n \in \mathcal{N} \tag{7}$$

where f_c denotes the carrier frequency.

The baseband channel model in (7) effectively consists of a time and a phase shift, both of which are caused by the physical propagation delay. Due to the time shift the received signal at different antennas can correspond to different transmit symbols. This effect is known as SWE [6]. Note that ignoring the time-shift, i.e., assuming $h_n(t) \approx e^{-j2\pi f_\mathrm{c}\tau_n}$, is known as *narrowband assumption*, which does not hold for the targeted wideband channels in the mmWave and sub-THz regime.

C. Beamformer

Because we consider a low-cost system, the receiver is assumed to be equipped with an analog PSN, i.e., a digitally controllable phase shift is applied to the received signal of each antenna before the signals of all antennas are superimposed in the analog domain. We assume phase shifters with infinite precision which realize pure phase shifts, i.e., they do not introduce any additional time delay[1]. The phase shift introduced by the nth phase shifter is denoted as $e^{j\psi_n}$, $n \in \mathcal{N}$. In order to compensate the phase shift which is introduced by the channel, the phase shift at the nth antenna is chosen to

$$\psi_n = 2\pi f_\mathrm{c} \tau_n. \tag{8}$$

Note that the PSN is not able to compensate any delays. Consequently, the signals of the different antennas are added up *incoherently* in the analog PSN, which introduces additional ISI. Fig. 3 illustrates this effect.

[1]This corresponds to reflection-type or vector modulator implementations.

D. Received Signal

Utilizing the FTN transmit signal from (3) and the wideband time domain channel model from (7), the received signal at the nth antenna is given by

$$\begin{aligned} \tilde{y}_n(t) &= x(t) * h_n(t) + \tilde{n}_n(t) \\ &= \sum_{l=1}^{m} x_l\, f\left(t - \frac{lT_\mathrm{s}}{M_\mathrm{Tx}} - \tau_n\right) e^{-j2\pi f_\mathrm{c}\tau_n} + \tilde{n}_n(t), \end{aligned} \tag{9}$$

where $\tilde{n}_n(t)$ denotes the AWGN process at the nth antenna. After beamforming and receive filtering by $g(t)$, the received signal is given by

$$\begin{aligned} y(t) &= \left(\sum_{n=1}^{N} \tilde{y}_n(t)\, e^{j\psi_n}\right) * g(t) \\ &= \sum_{l=1}^{m} x_l\, \bar{v}\left(t - \frac{lT_\mathrm{s}}{M_\mathrm{Tx}}\right) + \bar{n}(t) * g(t), \end{aligned} \tag{10}$$

with

$$\bar{n}(t) = \sum_{n=1}^{N} \tilde{n}_n(t)\, e^{j\psi(n)} \tag{11}$$

$$\bar{v}(t) = \sum_{n=1}^{N} v\left(t - \tau_n\right) \underbrace{e^{j(\psi_n - 2\pi f_\mathrm{c}\tau_n)}}_{=1}, \tag{12}$$

where $v(t) = f(t) * g(t)$ denotes the combined transmit and receive filter. $\bar{v}(t)$ can be understood as the *effective filter*, which captures the effects of beamforming and incoherent analog addition.

Sampling the received signal $y(t)$ with rate $M_\mathrm{Rx}/T_\mathrm{s}$, where M_Rx denotes the temporal oversampling factor w.r.t. the Nyquist rate, yields

$$y_k = \sum_{l=1}^{m} x_l\, \bar{v}\left(\frac{kT_\mathrm{s}}{M_\mathrm{Rx}} - \frac{lT_\mathrm{s}}{M_\mathrm{Tx}}\right) + \bar{n}\left(\frac{kT_\mathrm{s}}{M_\mathrm{Rx}}\right) * g\left(\frac{kT_\mathrm{s}}{M_\mathrm{Rx}}\right). \tag{13}$$

Afterwards, 1-bit quantization is applied independently to the real and imaginary part of the received signal, which yields

$$r_k = \mathcal{Q}_1\left(y_k\right) = p_k + jq_k, \tag{14}$$

with

$$p_k = \mathrm{sign}\left(\Re\{y_k\}\right), \quad q_k = \mathrm{sign}\left(\Im\{y_k\}\right), \tag{15}$$

where the real and imaginary operators are denoted by $\Re\{\cdot\}$ and $\Im\{\cdot\}$, respectively.

E. Generic Discrete Time System Model

Assuming an integer effective oversampling factor $M \in \mathbb{N}_+$ defined as $M = \frac{M_\mathrm{Rx}}{M_\mathrm{Tx}} \geq 1$, a generic discrete time system model can be obtained as

$$\mathbf{r}_k = \mathcal{Q}_1\left(\bar{\mathbf{V}}\mathbf{U}\mathbf{x}_{k-L}^{k} + \mathbf{n}_k\right), \tag{16}$$

where k denotes the transmit symbol index and we use the notation $\mathbf{x}_{k-L}^{k} = [x_{k-L}, \ldots, x_k]^T$. The vector $\mathbf{r}_k \in \mathbb{C}^M$ contains M complex 1-bit quantized samples which are associated with x_k, but also depend on the L previous transmit

This document is a preprint of: P. Neuhaus, M. Dorpinghaus, H. Halbauer et al., "Sub-THz Wideband System Employing 1-bit Quantization and Temporal Oversampling," in Proceedings of IEEE International Conference on Communications (ICC 2020), Dublin, Ireland, (pp. 1-7), Jun 2020. DOI:10.1109/ICC40277.2020.9148753

symbols. Hence, L is referred to as memory length (measured in transmit symbols) of the ISI channel. The effective filter matrix $\bar{\mathbf{V}} \in \mathbb{C}^{M \times M(L+1)}$ is a Toeplitz matrix defined as

$$\bar{\mathbf{V}} = \begin{bmatrix} \left[\ \bar{\mathbf{v}}_{\mathrm{r}}^T\ \right] & 0 \cdots & 0 \\ 0 & \left[\ \bar{\mathbf{v}}_{\mathrm{r}}^T\ \right] & 0 \cdots 0 \\ & \ddots\ \ddots\ \ddots & \\ 0 \cdots & 0 & \left[\ \bar{\mathbf{v}}_{\mathrm{r}}^T\ \right] \end{bmatrix}, \tag{17}$$

with

$$\bar{\mathbf{v}}_{\mathrm{r}}^T = \Bigg[\bar{v}\left(\frac{K}{2}\frac{T_{\mathrm{s}}}{M_{\mathrm{Rx}}}\right), \ldots, \bar{v}\left(\frac{T_{\mathrm{s}}}{M_{\mathrm{Rx}}}\right), \bar{v}\left(0\right), \bar{v}\left(-\frac{T_{\mathrm{s}}}{M_{\mathrm{Rx}}}\right), \ldots, \bar{v}\left(-\frac{K}{2}\frac{T_{\mathrm{s}}}{M_{\mathrm{Rx}}}\right)\Bigg], \tag{18}$$

where $K = LM$ is assumed to be even. Furthermore, $\mathbf{U} \in \mathbb{R}^{M(L+1) \times L+1}$ is an upsampling matrix which inserts $M-1$ zeros after each element of $\mathbf{x}_{k-L}^k$ and is defined as

$$[\mathbf{U}]_{i,j} = \begin{cases} 1, & \text{for } i = 1 + (j-1) \cdot M \\ 0, & \text{else,} \end{cases} \tag{19}$$

with $i \in \{1, \ldots, M(L+1)\}$, $j \in \{1, \ldots, L+1\}$. The AWGN noise process at the receiver is denoted by $\mathbf{n}_k$, which is correlated for $M_{\mathrm{Rx}} > 1$ because of receive filtering and temporal oversampling. For a RRC receive filter, the covariance matrix $\mathbf{\Sigma}_n$ of $\mathbf{n}_k$ is given by, cf. [18, eq. (9-2-27)],

$$[\mathbf{\Sigma}_n]_{i,j} = \sigma_n^2 \frac{\sin\left(\pi |i-j|/M_{\mathrm{Rx}}\right)}{\pi |i-j|/M_{\mathrm{Rx}}} \frac{\cos\left(\pi\beta |i-j|/M_{\mathrm{Rx}}\right)}{1-(2\beta |i-j|/M_{\mathrm{Rx}})^2}, \tag{20}$$

where β and $\sigma_n^2 = \frac{N_0}{T_{\mathrm{s}}}$ denote the rolloff factor and the noise variance, respectively. The combined receive vector after 1-bit quantization is defined as $\mathbf{r}^{\bar{m}} = \left[\mathbf{r}_1^T, \ldots, \mathbf{r}_m^T\right]^T$, with $\bar{m} = m\,M$.

For detection it is useful to convert the complex-valued generic discrete time system model from (16) to an equivalent real-valued system model as follows

$$\begin{bmatrix} \Re\{\mathbf{r}_k\} \\ \Im\{\mathbf{r}_k\} \end{bmatrix} = \begin{bmatrix} \mathbf{p}_k \\ \mathbf{q}_k \end{bmatrix} = \mathrm{sign}\left(\frac{1}{\sqrt{2}}\mathbf{V}\begin{bmatrix} \mathbf{a}_{k-L}^k \\ \mathbf{b}_{k-L}^k \end{bmatrix} + \begin{bmatrix} \Re\{\mathbf{n}_k\} \\ \Im\{\mathbf{n}_k\} \end{bmatrix}\right), \tag{21}$$

where

$$\mathbf{V} = \begin{bmatrix} \Re\{\bar{\mathbf{V}}\mathbf{U}\} & -\Im\{\bar{\mathbf{V}}\mathbf{U}\} \\ \Im\{\bar{\mathbf{V}}\mathbf{U}\} & \Re\{\bar{\mathbf{V}}\mathbf{U}\} \end{bmatrix}. \tag{22}$$

III. Encoding of Runlength-Limited Sequences

The maximum entropy, i.e., the capacity $C(d,k)$, of RLL codes is limited due to the (d,k) constraint [16]. RLL encoding is usually implemented using either block codes or FSM encoders. In this work we focus on the latter, because it enables code rates which are close to the capacity as well as it allows for efficient encoder and decoder implementations [19]. Note that RLL encoding using a FSM is somewhat similar to encoding of convolutional codes.

Table I: Finite-state machine encoder for $(1,\infty)$ RLL constraint with code rate $R_{\mathrm{RLL}} = 2/3$.

Current state	Input	Output	Next State
1	00	001	1
	01	010	2
	10	000	3
	11	010	3
2	00	100	2
	01	000	3
	10	100	3
	11	000	2
3	00	010	2
	01	010	3
	10	101	1
	11	001	1

Table II: Finite-state machine encoder for $(2,\infty)$ RLL constraint with code rate $R_{\mathrm{RLL}} = 1/2$.

Current state	Input	Output	Next State
1	0	00	3
	1	00	4
2	0	01	1
	1	00	3
3	0	01	1
	1	10	2
4	0	00	3
	1	00	4

Table III: Comparison of RLL finite state machine encoders.

RLL const. (d,k)	Capacity [16] $C(d,k)$ [bit/symbol]	FSM code rate R_{RLL} [bit/symbol]	Efficiency η
$(1,\infty)$	0.6942	2/3	0.96
$(2,\infty)$	0.5515	1/2	0.91

FSM encoders can be obtained from the RLL constraint definition (cf. Fig. 2) using the *ACH-algorithm*[2] [20]. The algorithm is graph-based and allows to construct FSM encoders with a rate $p/q < C(d,k)$, $p,q \in \mathbb{N}_+$. The construction starts with the constraint graph for all valid runs of length q. In each iteration a single node is split into two successors. The choice of node and edge splitting is guided by *approximate eigenvectors*. The algorithm terminates when each node in the graph has at least 2^p outgoing edges. The reader is referred to [19] for more details.

We derived two RLL FSM encoders for $d = 1$ and $d = 2$ using the ACH-algorithm, which are defined in Table I and Table II, respectively. Table III provides a comparison of the encoder parameters. The encoder efficiency $\eta = \frac{R_{\mathrm{RLL}}}{C(d,k)}$ measures how close the code rate of the encoder is to the capacity.

IV. Receiver

The receiver consists of 3 digital signal processing blocks (cf. Fig. 1): Firstly, the equalizer performs maximum a posteriori (MAP) symbol detection in order to equalize the ISI, which is caused by the effective filter and FTN signaling. The equalizer provides soft information, i.e., log-likelihood ratios (LLRs), for each RLL symbol. Note that obtaining soft-information is challenging after 1-bit quantization, however, it

[2]Also known as *state-splitting algorithm* [19].

is essential in order to profit from the performance of modern forward error correction (FEC) schemes. Secondly, the RLL decoder performs soft-input soft-output decoding of the RLL code. Finally, the FEC decoder decodes the channel code using soft information provided by the RLL decoder.

A. Soft-Ouput Equalizer

The MAP symbol detection problem for the equalizer can be formulated as

$$\hat{x}_k = \arg\max_{x_k \in \mathcal{X}} P\left(x_k|\mathbf{r}^{\bar{m}}\right). \tag{23}$$

For an efficient implementation, it is necessary to find a factorization of the a posteriori probability (APP) $P\left(\mathbf{x}^m|\mathbf{r}^{\bar{m}}\right)$. Using Bayes' theorem, it holds

$$P\left(\mathbf{x}^m|\mathbf{r}^{\bar{m}}\right) = \frac{P\left(\mathbf{r}^{\bar{m}}|\mathbf{x}^m\right)P\left(\mathbf{x}^m\right)}{P\left(\mathbf{r}^{\bar{m}}\right)}. \tag{24}$$

The a priori probability $P\left(\mathbf{x}^m\right)$ can be factorized as

$$\begin{aligned} P\left(\mathbf{x}^m\right) &= P\left(\mathbf{a}^m\right)P\left(\mathbf{b}^m\right) \\ &= \prod_{k=1}^{m} P(a_k|\mathbf{a}^{k-1})P(b_k|\mathbf{b}^{k-1}), \end{aligned} \tag{25}$$

where $P(a_k|\mathbf{a}^{k-1})$ and $P(b_k|\mathbf{b}^{k-1})$ can be obtained from the state transition probability of the underlying RLL sequence.

In order to obtain a tractable factorization for $P\left(\mathbf{r}^{\bar{m}}|\mathbf{x}^m\right)$, the temporal noise correlation between received signal vectors corresponding to different transmit symbols, e.g., between $\mathbf{r}_k$ and $\mathbf{r}_{k+1}$, is neglected. Then, $P\left(\mathbf{r}^{\bar{m}}|\mathbf{x}^m\right)$ can be factorized as

$$P\left(\mathbf{r}^{\bar{m}}|\mathbf{x}^m\right) = P\left(\mathbf{p}^{\bar{m}}|\mathbf{x}^m\right)P\left(\mathbf{q}^{\bar{m}}|\mathbf{x}^m\right) \tag{26}$$

$$\approx \prod_{k=1}^{m} P\left(\mathbf{p}_k|\mathbf{x}^k\right)P\left(\mathbf{q}_k|\mathbf{x}^k\right), \tag{27}$$

where

$$P\left(\mathbf{p}_k|\mathbf{x}^k\right) = \int_{\mathcal{P}_k^M} P\left(\mathbf{z}_k|\mathbf{x}^k\right)\mathrm{d}\mathbf{z}_k. \tag{28}$$

Therein $\mathbf{z}_k$ denotes the real part of the quantizer input, the integration region $\mathcal{P}_k^M = \mathcal{P}_{k,1} \times \ldots \times \mathcal{P}_{k,M}$ is defined by the output of the quantizer according to

$$\mathcal{P}_{k,m} = \begin{cases} (-\infty, 0), & \text{for } p_{k,m} = -1 \\ [0, \infty), & \text{for } p_{k,m} = +1, \end{cases}, \quad m \in \{1, \ldots, M\}, \tag{29}$$

and the probability density function (PDF) $P\left(\mathbf{z}_k|\mathbf{x}^k\right)$ is given by

$$\begin{aligned} P\left(\mathbf{z}_k|\mathbf{x}^k\right) &= \frac{1}{\sqrt{\pi^M\left|\mathbf{\Sigma}_n\right|}} \\ &\times \exp\left(-\left(\mathbf{z}_k - \boldsymbol{\mu}_{\mathrm{R}}(\mathbf{x}^k)\right)^T \mathbf{\Sigma}_n^{-1}\left(\mathbf{z}_k - \boldsymbol{\mu}_{\mathrm{R}}(\mathbf{x}^k)\right)\right), \end{aligned} \tag{30}$$

with mean

$$\boldsymbol{\mu}_{\mathrm{R}}(\mathbf{x}^k) = \frac{1}{\sqrt{2}}\begin{bmatrix}\Re\{\bar{\mathbf{V}}\mathbf{U}\} & -\Im\{\bar{\mathbf{V}}\mathbf{U}\}\end{bmatrix}\begin{bmatrix}\mathbf{a}_{k-L}^k \\ \mathbf{b}_{k-L}^k\end{bmatrix}. \tag{31}$$

$P\left(\mathbf{q}_k|\mathbf{x}^k\right)$ is defined similarly. Inserting (25) and (27) into (24) yields the APP factorization

$$P\left(\mathbf{x}^m|\mathbf{r}^{\bar{m}}\right) \approx \frac{\prod_{k=1}^{m} P\left(\mathbf{p}_k|\mathbf{x}^k\right)P\left(\mathbf{q}_k|\mathbf{x}^k\right)P(a_k|\mathbf{a}^{k-1})P(b_k|\mathbf{b}^{k-1})}{P\left(\mathbf{r}^{\bar{m}}\right)}. \tag{32}$$

1) BCJR Algorithm: MAP symbol detection can efficiently be implemented using the BCJR algorithm [21]. The algorithm works on a trellis, where each state $s_k \in \mathcal{S}$ at time instant k is defined by the previous real and imaginary input of memory length L, such that

$$s_{k-1} \triangleq \begin{bmatrix}\mathbf{a}_{k-L}^{k-1} \\ \mathbf{b}_{k-L}^{k-1}\end{bmatrix}. \tag{33}$$

Because of QPSK symbols the number of trellis states $|\mathcal{S}|$ is limited by $|\mathcal{S}| \leq 4^L$. Omitting states which correspond to sequences $\mathbf{a}_{k-L}^{k-1}$ and $\mathbf{b}_{k-L}^{k-1}$ which violate the RLL constraint allows to reduce the number of states for $d > 0$. The state transition probability $\gamma_k(s_{k-1}, s_k)$ between two states $s_{k-1}, s_k \in \mathcal{S}$ at time instant k depends on the observations $\mathbf{r}_k$ and is defined as

$$\gamma_k(s_{k-1}, s_k) = P(\mathbf{r}_k|s_{k-1}, s_k)P(s_k|s_{k-1}) \tag{34}$$

$$\approx P\left(\mathbf{p}_k|\mathbf{x}^k\right)P\left(\mathbf{q}_k|\mathbf{x}^k\right)P(a_k|\mathbf{a}^{k-1})P(b_k|\mathbf{b}^{k-1}), \tag{35}$$

where (35) is due to (27). Utilizing (34), the BCJR algorithm performs forward and backward recursions through the trellis, which are defined as

$$\alpha(s_k) = \sum_{s_{k-1} \in \mathcal{S}} \alpha(s_{k-1})\gamma_k(s_{k-1}, s_k) \tag{36}$$

and

$$\beta(s_k) = \sum_{s_{k+1} \in \mathcal{S}} \beta(s_{k+1})\gamma_{k+1}(s_k, s_{k+1}), \tag{37}$$

respectively. Note that the recursions have to be initialized appropriately, e.g., by starting and terminating in known states. A factorization of the joint probability can be obtained by combining (34), (36) and (37) to

$$P(s_{k-1}, s_k, \mathbf{r}^{\bar{m}}) = \alpha(s_{k-1})\gamma_k(s_{k-1}, s_k)\beta(s_k). \tag{38}$$

Let the sets $\mathcal{S}_a^+$ and $\mathcal{S}_a^-$ define the state pairs (s_{k-1}, s_k) which result in a transmit symbol at time index k of $a_k = +1$ and $a_k = -1$, respectively. Similar definitions hold for $\mathcal{S}_b^+$ and $\mathcal{S}_b^-$ with respect to b_k. Then, the joint probability in (38) can be used to compute logarithmic APP (log-APP) ratios

$$L(a_k) = \log\frac{\sum_{(s,s')\in\mathcal{S}_a^+} P(s_{k-1} = s, s_k = s', \mathbf{r}^{\bar{m}})}{\sum_{(s,s')\in\mathcal{S}_a^-} P(s_{k-1} = s, s_k = s', \mathbf{r}^{\bar{m}})}, \tag{39}$$

which provides soft information for each RLL encoded bit of the real part. Log-APP ratios for the imaginary part can be obtained similarly. Both sequences can be processed independently afterwards. Note that the proposed equalizer is somewhat similar to the *quantized BCJR* [15]. However, the proposed equalizer uses the RLL constraint to reduce the number of trellis states and transitions and also allows for temporal oversampling.

This document is a preprint of: P. Neuhaus, M. Dorpinghaus, H. Halbauer et al., "Sub-THz Wideband System Employing 1-bit Quantization and Temporal Oversampling," in Proceedings of IEEE International Conference on Communications (ICC 2020), Dublin, Ireland, (pp. 1-7), Jun 2020. DOI:10.1109/ICC40277.2020.9148753

Table IV: Extended FSM encoder for joint RLL and NRZI encoding derived from the RLL encoder defined in Table II.

Current state	Input	Output	Next State
1_+	0	$+1+1$	3_+
	1	$+1+1$	4_+
2_+	0	$+1-1$	1_-
	1	$+1+1$	3_+
3_+	0	$+1-1$	1_-
	1	$-1-1$	2_-
4_+	0	$+1+1$	3_+
	1	$+1+1$	4_+
1_-	0	$-1-1$	3_-
	1	$-1-1$	4_-
2_-	0	$-1+1$	1_+
	1	$-1-1$	3_-
3_-	0	$-1+1$	1_+
	1	$+1+1$	2_+
4_-	0	$-1-1$	3_-
	1	$-1-1$	4_-

B. Soft-Input Soft-Output Decoding of RLL Codes

We propose to implement joint soft-input soft-ouput NRZI and RLL decoding, which can be implemented efficiently using an extended version of the FSM representation of the encoders. For each state in the original FSM, the extended FSM contains two states, each of which is associated with the current sign of the RLL sequence, i.e., $+1$ or -1, which is denoted as $(\cdot)_+$ and $(\cdot)_-$, respectively. The output is computed by NRZI encoding using the sign which is associated with the current state. An example for the extended FSM which is derived from the FSM encoder of Table II is provided in Table IV. This approach avoids to compute soft-information for transitions, i.e., by soft-input soft-output NRZI decoding, at the cost of doubling the number of states and transitions in the FSM decoder. Since both FSM encoders have a small number of states the resulting size of the extended FSMs, i.e., 6 and 8 states, is still low. Joint soft-input soft-output NRZI and RLL decoding can then straightforwardly be implemented on the extended FSM using the BCJR algorithm [21].

V. Numerical Results

Numerical results in this section are obtained assuming RRC transmit and receive filters with a bandwidth $\frac{1+\beta}{T_\mathrm{s}}$, a rolloff of $\beta = 1$, and truncation after 100 Nyquist intervals. The effective filter in the equalizer is truncated once the coefficients fall below $5\,\%$ of the maximum using an auxiliary channel law, similar to [22]. The RLL constraint is always chosen as $(d = M_\mathrm{Tx} - 1, k = \infty)$. This choice ensures a minimum distance of T_s between two zero crossings which enables the continuous-time transmit waveform to reach its full amplitude between all transitions. We expect that this choice enhances the system's robustness against noise. The performance is evaluated for the lowest new unlicensed FCC band with a carrier frequency $f_\mathrm{c} = 119.5\,\mathrm{GHz}$ and a bandwidth of $\frac{1}{T_\mathrm{s}} = 7\,\mathrm{GHz}$ [23]. The URA at the receiver is assumed to be of size $N_\mathrm{h} = N_\mathrm{v} = 8$, with antenna spacing $d_\mathrm{h} = d_\mathrm{v} = \frac{\lambda_\mathrm{c}}{2}$, where $\lambda_\mathrm{c} = \frac{c}{f_\mathrm{c}}$, such that it consists of $N = 64$ antennas. The azimuth and elevation AoAs are assumed to be uniformly distributed over $[-\frac{\pi}{3}, \frac{\pi}{3}]$. The channel and beamformer are normalized such that both result in unit gain, i.e., there is no path loss and no beamforming gain. We evaluate the average performance for $4 \cdot 10^3$ independent realizations of ϕ and θ. As FEC scheme we employ the 5G NR LDPC code from the *MATLAB 5G Toolbox*, including cyclic redundancy check (CRC) coding, code block segmentation, rate matching, and rate recovery. All results are obtained for the LDPC base graph 1 and an information block size of $K_\mathrm{FEC} = 8448$ at the FEC encoder input.

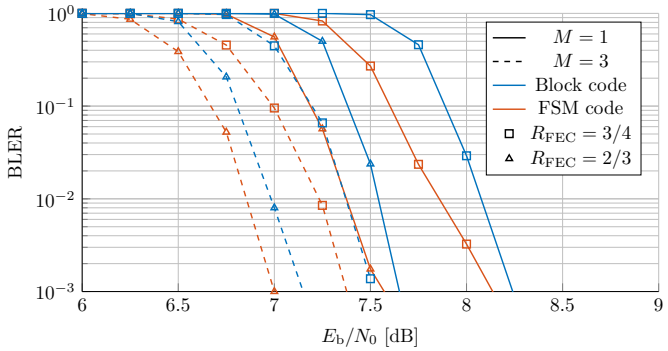

Fig. 4. Performance comparison of proposed $d = 1$ RLL FSM code from Tab. I and block code from [16, Tab. 4] for $M_\mathrm{Tx} = 2$.

A. Comparison of Proposed RLL FSM to RLL Block Code

First we compare the performance of the proposed FSM RLL code from Tab. I to a well known fixed length RLL block code with a constraint of $(1, \infty)$ and a rate of $R_\mathrm{RLL} = 0.6$ from [16, Tab. 4]. The code achieves an efficiency of $\eta = \frac{R_\mathrm{RLL}}{C(1,\infty)} \approx 0.86$ and is therefore $10\,\%$ less efficient than the propose FSM code (cf. Tab. III). Soft demapping is performed by first computing the probability of each RLL code word conditioned on the input. From these it is straightforward to compute LLRs for each encoded information bit. The performance of both codes is evaluated with respect to the block-error ratio (BLER) in Fig. 4. The proposed FSM code outperforms the block code by approx. $0.1\,\mathrm{dB}$ to $0.2\,\mathrm{dB}$ at a BLER of 10^{-2} although it achieves a higher rate.

B. Coded System Performance Evaluation with FSM Codes

The gain of oversampling w.r.t. the signaling rate is investigated in Fig. 5 for $M_\mathrm{Tx} = 2$. Increasing M_Rx from sampling at signaling rate to 3-fold oversampling w.r.t. the signaling rate, i.e., from $M = 1$ to $M = 3$, yields approx. $0.5\,\mathrm{dB}$ to $0.8\,\mathrm{dB}$ gain at a BLER of 10^{-2}. The gain decreases slightly with decreasing code rate. Furthermore, oversampling increases the slope of decay for $R_\mathrm{FEC} \in \{\frac{4}{5}, \frac{8}{9}\}$.

The performance for different FTN signaling rates M_Tx is compared in Fig. 6. Increasing the signaling rate requires approx. $1.3\,\mathrm{dB}$ to $2.3\,\mathrm{dB}$ increase in E_b/N_0 in order to achieve a similar performance at a BLER of 10^{-2}. Results are less smooth and steep for $M_\mathrm{Tx} = 3$ and $R_\mathrm{FEC} \in \{\frac{4}{5}, \frac{8}{9}\}$, which could be caused by increased ISI. Regarding the shown number of information bits per Nyquist interval note that the resulting spectral efficiency also depends on the power spectral density of the RLL sequence, which becomes more narrow for increased d constraints [16].

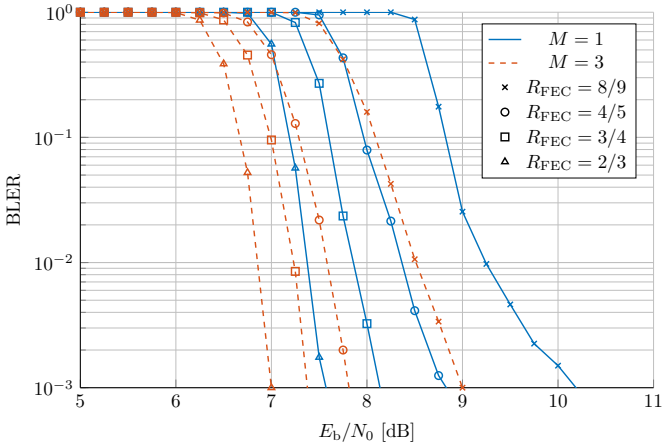

Fig. 5. Performance evaluation of oversampling for $M_{\mathrm{Tx}} = 2$ using the proposed FSM code with $d = 1$.

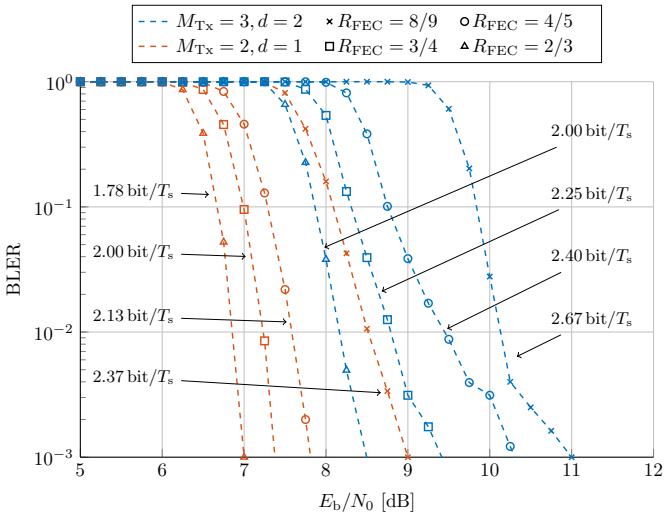

Fig. 6. Performance comparison of FTN signaling factors M_{Tx} for $M = 3$ using the proposed FSM codes with $d = 1$ and $d = 2$. Arrows indicate the number of information bits which can be transmitted per Nyquist interval T_{s}. For the considered frequency band, $2\,\mathrm{bit}/T_{\mathrm{s}}$ corresponds to a data rate of $14\,\mathrm{Gbit/s}$.

VI. Conclusions

In this work we proposed two FSM RLL codes for an efficient implementation of ZXM. The performance of the proposed FSM RLL code with constraint $(d = 1, k = \infty)$ was found to be superior as compared to a standard block code. Utilizing these codes in combination with FTN signaling and temporal oversampling, we proposed a system which is able to obtain soft information at the receiver after 1-bit quantization. The coded performance of the proposed sub-THz system has then been evaluated for a wideband LOS channel. An extension to more realistic channel models remains open.

Acknowledgment

This work is supported in part by the Deutsche Forschungsgemeinschaft (DFG, German Research Foundation) – Project-ID 164481002 – SFB 912, HAEC. Computations were performed at the Center for Information Services and High Performance Computing (ZIH) at TU Dresden.

References

[1] T. S. Rappaport, Y. Xing, O. Kanhere, S. Ju, A. Madanayake, S. Mandal, A. Alkhateeb, and G. C. Trichopoulos, “Wireless communications and applications above 100 GHz: Opportunities and challenges for 6G and beyond,” *IEEE Access*, vol. 7, pp. 78 729–78 757, 2019.

[2] S. Krone and G. Fettweis, “Energy-efficient A/D conversion in wideband communications receivers,” in *Proc. IEEE Veh. Technol. Conf. (VTC Fall)*, San Francisco, CA, USA, Sept. 2011, pp. 1–5.

[3] R. B. Staszewski, “Digitally intensive wireless transceivers,” *IEEE Des. Test of Comput.*, vol. 29, no. 6, pp. 7–18, Dec. 2012.

[4] S. Ziabakhsh, G. Gagnon, and G. W. Roberts, “The peak-SNR performances of voltage-mode versus time-mode circuits,” *IEEE Trans. Circuits Syst., II, Exp. Briefs*, vol. 65, no. 12, pp. 1869–1873, Dec. 2018.

[5] G. Fettweis, M. Dörpinghaus, S. Bender, L. Landau, P. Neuhaus, and M. Schlüter, “Zero crossing modulation for communication with temporally oversampled 1-bit quantization,” in *Proc. Asilomar Conf. on Signals, Systems, and Computers*, Pacific Grove, CA, USA, Nov. 2019.

[6] B. Wang, F. Gao, S. Jin, H. Lin, and G. Y. Li, “Spatial- and frequency-wideband effects in millimeter-wave massive MIMO systems,” *IEEE Trans. Signal Process.*, vol. 66, no. 13, pp. 3393–3406, July 2018.

[7] L. T. N. Landau, M. Dörpinghaus, and G. P. Fettweis, “1-bit quantization and oversampling at the receiver: Sequence-based communication,” *EURASIP J. Wireless Commun. Netw.*, vol. 2018, no. 1, p. 83, 2018.

[8] S. Bender, M. Dörpinghaus, and G. Fettweis, “On the achievable rate of bandlimited continuous-time 1-bit quantized AWGN channels,” in *Proc. IEEE Int. Symp. on Inf. Theory (ISIT)*, Aachen, Germany, June 2017, pp. 2083–2087.

[9] ——, “On the achievable rate of multi-antenna receivers with oversampled 1-bit quantization,” in *Proc. IEEE Int. Workshop on Comput. Advances in Multi-Sensor Adaptive Process. (CAMSAP)*, Curaçao, Dutch Antilles, Dec. 2017, pp. 1–5.

[10] M. Schlüter, M. Dörpinghaus, and G. P. Fettweis, “On the timing synchronization under 1-bit quantization and oversampling,” in *Proc. IEEE Statistical Signal Process. Workshop (SSP)*, Freiburg, Germany, June 2018, pp. 198–202.

[11] ——, “Bounds on channel parameter estimation with 1-bit quantization and oversampling,” in *Proc. IEEE Int. Workshop on Signal Process. Advances in Wireless Commun. (SPAWC)*, Kalamata, Greece, June 2018.

[12] ——, “Bounds on phase and frequency estimation from 1-bit quantized signals with phase dithering,” in *Proc. IEEE Int. Conf. on Commun. (ICC)*, Shanghai, China, May 2019, pp. 1–6.

[13] P. Neuhaus, M. Dörpinghaus, and G. Fettweis, “Oversampled 1-bit quantized wideband systems: Is it better to spend samples in time or in space?” in *Proc. IEEE Int. Workshop on Signal Process. Advances in Wireless Commun. (SPAWC)*, Cannes, France, July 2019, pp. 1–5.

[14] A. Gokceoglu, E. Björnson, E. G. Larsson, and M. Valkama, “Spatio-temporal waveform design for multiuser massive MIMO downlink with 1-bit receivers,” *IEEE J. Sel. Topics Signal Process.*, vol. 11, no. 2, pp. 347–362, Mar. 2017.

[15] Y. Jeon, H. Do, S. Hong, and N. Lee, “Soft-output detection methods for sparse millimeter-wave MIMO systems with low-precision ADCs,” *IEEE Trans. Commun.*, vol. 67, no. 4, pp. 2822–2836, Apr. 2019.

[16] K. A. S. Immink, “Runlength-limited sequences,” *Proc. IEEE*, vol. 78, no. 11, pp. 1745–1759, Nov. 1990.

[17] J. E. Mazo, “Faster-than-Nyquist signaling,” *Bell Syst. Tech. J.*, vol. 54, no. 8, pp. 1451–1462, Oct. 1975.

[18] J. G. Proakis, *Digital Communications*. New York, USA: McGraw-Hill, 1995.

[19] B. H. Marcus, R. M. Roth, and P. H. Siegel, “An introduction to coding for constrained systems,” *Lecture notes*, 2001.

[20] R. Adler, D. Coppersmith, and M. Hassner, “Algorithms for sliding block codes - an application of symbolic dynamics to information theory,” *IEEE Trans. Inf. Theory*, vol. 29, no. 1, pp. 5–22, Jan. 1983.

[21] L. Bahl, J. Cocke, F. Jelinek, and J. Raviv, “Optimal decoding of linear codes for minimizing symbol error rate (corresp.),” *IEEE Trans. Inf. Theory*, vol. 20, no. 2, pp. 284–287, Mar. 1974.

[22] L. Landau, M. Dörpinghaus, and G. P. Fettweis, “1-bit quantization and oversampling at the receiver: Communication over bandlimited channels with noise,” *IEEE Commun. Lett.*, vol. 21, no. 5, pp. 1007–1010, May 2017.

[23] FCC 19-19, “Part of docket no. 18-21. first report and order,” https://ecfsapi.fcc.gov/file/0321900915630/FCC-19-19A1.pdf, Mar. 2019.